IMAGE RECONSTRUCTION USING WAVELET TRANSFORM

by

G. VARADARAJAN

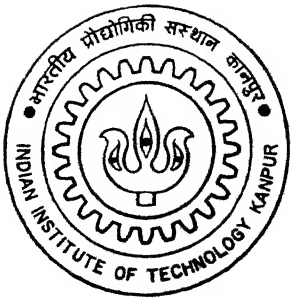

DEPARTMENT OF ELECTRICAL ENGINEERING

INDIAN INSTITUTE OF TECHNOLOGY KANPUR

JANUARY, 1995

IMAGE RECONSTRUCTION USING WAVELET TRANSFORM

A Thesis Submitted
in Partial Fulfilment of the Requirements
for the Degree of
MASTER OF TECHNOLOGY

by

G.VARADARAJAN

to the
DEPARTMENT OF ELECTRICAL ENGINEERING
INDIAN INSTITUTE OF TECHNOLOGY KANPUR

January 1995

CERTIFICATE

It is certified that the work contained in the thesis titled Image Reconstruction Using Wavelet Transform, by G.Varadarajan has been carried out under my supervision and that this work has not been submitted elsewhere for a degree.

January, 1995

Dr.Sumana Gupta
Associate Professor,
Department of Electrical Engineering
IIT, Kanpur.

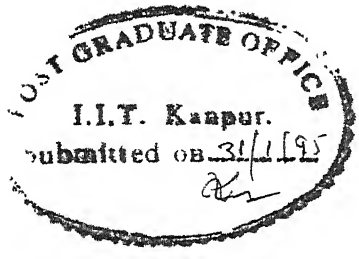

ABSTRACT

In this thesis work some applications of Wavelet transform in the area of Image Reconstruction from Projections have been studied. The process of data collection in computer aided tomography, introduces noise in the projections. One of the major sources of noise is the statistical nature of photon emission and detection. The wavelet transform is used to reduce the effect of noise in the reconstructed image by preprocessing the noisy projections. This method is compared with the existing technique and its advantages and disadvantages are discussed. It is shown that reconstruction of images from the 1D wavelet transform of the projections gives the 2D wavelet transform of the original image. The 2D wavelet corresponding to this wavelet transform is shown to be the inverse Radon transform of the 1D wavelet. These two results are combined to produce the noise suppressed analysis images from the noisy projections. The above results are verified through simulations using computer generated images.

To,

All those

who helped me

to be

what I am today

Acknowledgement

I would like to express my deep sense of gratitude to my thesis supervisor Dr. Sumana Gupta for the help and guidance I received in the course of my thesis work. I thank her for allowing me to work in the area of my interest and helping me out whenever I run into trouble. I am indebted to Dr. Rathore for sparing his valuable time to clear my doubts. I would like to thank Dr. S.K.Mullick, Dr P.R.K.Rao and Dr. M.U.Siddiqui for introducing me to various interesting fields during my course work. The informal discussions I had with Dr. P.R.K.Rao, were thought provoking and will linger in my memory long after I am gone from this place.

I thank Johnson for running around with me for various thesis report related work. Without his help, my thesis submission would have got considerably delayed. I thank Cheenu for guiding me through xfig and Kumar for his timely helps. I thank all those who helped in making the life in the hostel a bit more easier and enjoyable. It is extremely difficult to find words to thank the other four members of the G5(Kamat,Venu,Pai and Bhavesh). Their support to me through the 18 months of my stay here, cannot be acknowledged in a few words. Words do fail me!

Contents

Chapter 1

Introduction

1.1 Review

The problem of determining some property of the internal structure of some object without macroscopically damaging the object arises in diverse area such as medicine, electron microscopy, stress analysis etc. Radon transform is the unifying mathematical framework for all such problems. In medicine, X-ray transmission tomography, also known as computer tomography(CT), is one of the important techniques used to obtain the x-ray attenuation coefficient distribution over a cross section of some portion of the human body from the projection profile that are measured at various angles. The process of collecting projection data has many practical limitations, thereby, introducing error in the projection measurements. One such basic limitation to the accuracy of measurements in CT is the statistical nature of the photon production, its interaction with the matter and photon detection [3]. It is shown that this error can be modeled as Additive Gaussian noise with zero mean [13]. At high frequency, this noise dominates the signal. The reconstruction process, which involves filtering the projection with ramp filter, amplifies the high frequency content of the input signal. This effectively increases the noise in the reconstructed image. In practice this problem is tackled by using a lowpass filter in conjunction with the ramp filter. This low pass filter will have gentle roll off characteristic to avoid ringing. The problem with this spatially invariant filtering is, it suppresses the high frequency content of the signal along with the noise. Thus the improvement in noise performance comes at the expense of resolution.

Recently a few methods using spatially variant filtering have been proposed in the lit-

erature [9, 10]. In [9], Sahiner et.al., propose a spatially varying filtering using time frequency distribution. Window Fourier transform is used to represent the signal in the time-frequency plane. In [10], the same authors propose a method using wavelets, where prior knowledge of the image is used to set some of the coefficients of the 2D wavelet transform of the image to zero and reconstruct the image imposing these constraints.

One major problem in window Fourier transform is in choosing an appropriate window (the analysis filter). Too short a window may result in poor frequency resolution and too long may result in poor spatial resolution. This problem does not arise if we choose wavelet transform instead of window Fourier transform, because in wavelet transform, the window size varies as a function of scale. Also fast algorithms exist in computing the wavelet transform. With this as motivation we propose a method using spatially varying filtering in time-frequency plane using wavelet transform. Unlike in [10], we assume no prior knowledge of the original image.

Wavelet transform of a given signal can be expressed as convolution of the given signal with $\psi_a(-s)$, the reversed wavelet at a given scale 'a' , where $\psi(s)$ is an admissible one dimensional wavelet[5]. From the convolution property of the Radon transform, we know that the Radon transform of the two dimensional convolution of two signals is the same as the one dimensional convolution of the Radon transform of the two signals on the variable 's' [1]. Using this property it can be shown that the reconstructed images from the wavelet transform of its projections can be said to be two dimensional convolution of the original 2D image with a 2 dimensional function $\Psi_a(-x,-y)$ which is the inverse Radon Transform of the one dimensional analysing wavelet (rather its reflected and scaled version, to be precise). We show in this work that the two dimensional function $\Psi_a(-x,-y)$ is a reversed and scaled version of a two dimensional function i.e., $\Psi_a(-x,-y) = \Psi(-x/a,-y/a)$. We also show that $\Psi(x,y)$ is an admissible two dimensional wavelet [12].

1.2 Organization of Thesis

- In chapter 2, we review the relevant results in Radon transform, Wavelet transform and Detection theory.

- In chapter 3, we propose a method to suppress noise in the reconstructed image from noisy projections using wavelet transform.
- In chapter 4, we prove that $\Psi(x, y)$ is an admissible wavelet and hence show that the 2 dimensional convolution is actually the 2 dimensional wavelet transform equation.
- We test the above propositions on computer simulated projections of the synthetic images and present the results in chapter 5.
- Suggestion for future work is presented in chapter 6.
- We summarise our results and conclude in chapter 7.

In this thesis work we use $\mathcal{R}$ to represent the set of real numbers and $\mathcal{Z}$ to represent the set of integers.

Chapter 2

Mathematical Preliminaries

In this chapter a very brief review of the results that will be used in this work are given. We direct the interested reader to texts and journal articles, for a detailed treatment on these topics. These references are listed in Bibliography. In section 1 we review Radon transform and some of its properties. In section 2, we present the relevant results in wavelet transform and multiresolution analysis. In section 3, we give two results from detection theory which will be used in this work.

2.1 Radon Transform

Image reconstructions from projections is the process of producing an image of a two dimensional distribution (of some physical property) from the estimates of its line integral along a finite number of lines of known locations. The basic mathematical framework common to a large class of such reconstruction problem was first developed by Johann Radon as early as in 1917. His work which has come to be known as Radon transform on Euclidean space ($\mathcal{R}^n$), relates a function defined on n-dimensional Euclidean space $\mathcal{R}^n$ and its integrals over all the hyperplanes of dimension n-1. Thus if f is defined over a plane $\mathcal{R}^2$, like in 2 dimensional medical imaging, its Radon transform is determined by its line integrals over all lines passing through the function support. Knowledge of all possible line integrals constitute full knowledge of the Radon transform. In Practice we have only a finite number of samples of the Radon transform. The image reconstruction techniques deal with the problem of reconstructing the image from this partial information.

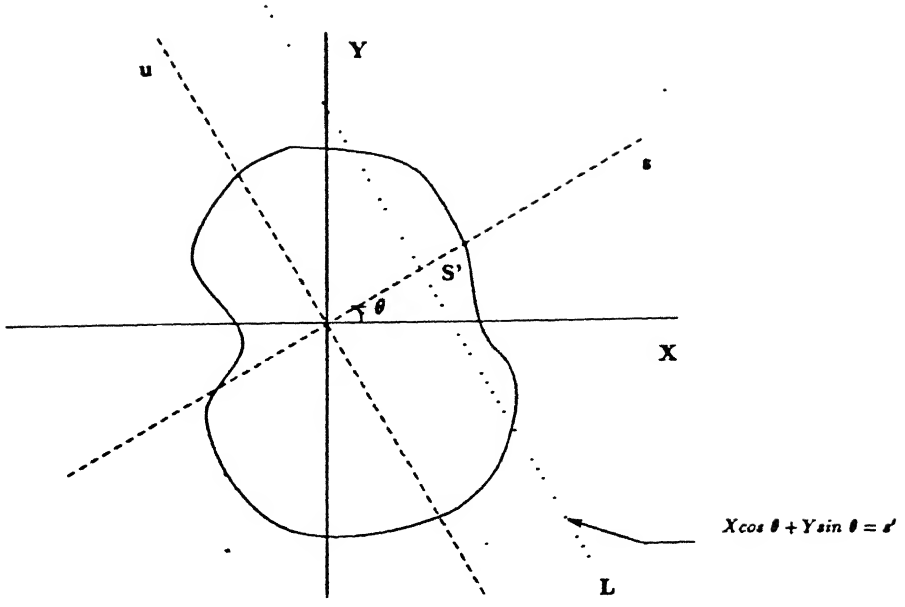

Figure 2.1: *The coordinates in space domain and the line L representing the line of integration*

Definition : Let (x, y) designate coordinates of a point in a plane. Consider an arbitrary function $f(x, y)$ defined over some domain D in R^2. Then its Radon transform (also known as the projections), $g(s, \theta)$ is given by

$$g(s,\theta) = \int_{-\infty}^{\infty} \int_{-\infty}^{\infty} f(x,y)\delta(x cos\theta + y sin\theta - s)\, dx\, dy \tag{2.1}$$

If f is continuous and has compact support, then $g(s, \theta)$ uniquely determines $f(x, y)$ [1].

In equation 2.1, $\delta(.)$ is a Dirac Delta function.Thus for a given θ, the equation 2.1 is a line integral along the line $x\cos\theta + y\sin\theta = s$ (figure 2.1). Associated with Radon transform is the Back projection operator which is given by

$$b(x,y) = \int_0^{\pi} g(x\cos\theta + y\sin\theta, \theta)\, d\theta \tag{2.2}$$

Back projection represents the accumulation of the ray sums of all the rays that pass through the point (x, y). Backprojection operator is not the inverse of the Radon transform but the inverse Radon transform operation involves this operator. The inverse Radon

transform is,

$$f(x,y) = \frac{1}{4\pi^2} \int_0^{\pi} \int_{-\infty}^{\infty} |\xi| \, \hat{g}(\xi,\theta) \, e^{j\xi(x\cos\theta + y\sin\theta)} \, d\xi \, d\theta \tag{2.3}$$

where $\hat{g}(\xi,\theta)$ is the one dimensional Fourier transform of $g(s,\theta)$ with respect to 's'. We note that in equation 2.3, the inner integral represents the inverse Fourier transform of $|\xi|\hat{g}(\xi,\theta)$, i.e., it represents the filtering of the projections $g(s,\theta)$ with the ramp filter $p(s)$ whose frequency response is $|\xi|$. The outer integral represents the backprojection operation on these filtered projection.

As mentioned in chapter 1, the ramp filter amplifies the high frequency components of the projections. Since the noise strength in the high frequency region is generally more than the signal strength, it is common practice to use a low pass filter $\hat{w}(\xi)$ in conjunction with the ramp filter, to improve signal to noise ratio. Hence the filter $|\xi|$ in equation 2.3 is replaced by $\hat{h}(\xi) = |\xi|\hat{w}(\xi)$. The low pass filter usually has a gentle roll off characteristics to avoid ringing at the edges. One such filter $\hat{h}(\xi)$, which exhibits good noise suppressing property is [2, 13],

$$\hat{h}(\xi) = |\xi| \, [\alpha + (1-\alpha)\cos 2\pi\xi d] \text{ for } |\xi| \leq 1/2d \tag{2.4}$$

where d is the sampling interval along the variable 's'. This filter is called generalized Hamming filter. But this space invariant lowpass filtering results in loss of resolution, since the filter $\hat{h}(\xi)$ smoothes out the edges in the image. We will come back to this problem in chapter 3.

Some properties of the Radon transform which we will refer to in this work are given below. In the following properties $g(s,\theta)$, $g_1(s,\theta)$ and $g_2(s,\theta)$ represent the Radon transform of the functions $f(x,y)$, $f_1(x,y)$ and $f_2(x,y)$ respectively. $\hat{g}(\xi,\theta)$ is the Fourier transform of $g(s,\theta)$ and $\hat{F}(\xi_1,\xi_2)$ is the 2 dimensional Fourier transform of $f(x,y)$.

1. *Projection Slice theorem :* The one dimensional Fourier transform on s of $g(s,\theta)$ is equal to the central slice, at an angle θ of the 2 dimensional Fourier transform of the object $f(x,y)$.

$$\hat{g}(\xi,\theta) = \hat{F}(\xi\cos\theta, \xi\sin\theta) \tag{2.5}$$

2. Radon transform is linear, i.e., given the scalars, $a_1, a_2 \in \mathcal{R}$, we have,

$$a_1 f_1(x,y) + a_2 f_2(x,y) \xleftrightarrow{\text{R.T}} a_1 g_1(s,\theta) + a_2 g_2(s,\theta)$$

3. *Convolution property :* The Radon transform of the 2 dimensional convolution of two 2-D signals $f_1(x,y)$ *and* $f_2(x,y)$ is the 1 dimensional convolution of the Radon transform of the two signals.

$$f_1(x,y) \otimes_2 f_2(x,y) \overset{\text{R.T.}}{\longleftrightarrow} g_1(s,\theta) \otimes_1 g_2(s,\theta) \tag{2.6}$$

where $\otimes_1$ represents one dimensional convolution on 's', $\otimes_2$ represents two dimensional convolution and R.T represents the Radon transform operation.

In Computer Tomography, the linear attenuation coefficient, $\mu(x,y)$, of the material to x-ray is the quantity we are trying to estimate. We use the data collected through x-rays which gives an estimate of the line integrals.

$$\int_L \mu(x,y)\, du = -\ln\left(\frac{I}{I_0}\right)$$

where I_0 is the input intensity (number of photons per sec per unit area), I is the observed intensity after the beam passes through the material and du is the increment length along the line L (figure 2.1). In actual measurement due to practical limitations such as the statistical nature of the photon emission and detection, beam hardening etc.[3] noise is added to the projections. In [13] Shepp et al., show that noise introduced due to the statistical nature of photon can be modelled as an additive Gaussian noise with zero mean.

Proofs of the above properties, are given in [1, 2]. The computer implementation of discretized reconstruction algorithm is discussed in detail by Rowland in [4]. In [3], Herman presents a detailed discussion of various reconstruction techniques as related to computer tomography and its practical limitations. For an overview of Radon transform, its properties and an English translation of Radon's original paper, refer [1].

2.2 Wavelet Transform

Wavelets are relatively recent development in applied mathematics. The concept of wavelets can be viewed as a synthesis of ideas which originated in diverse areas such as, physics, engineering, and pure mathematics. As a result, wavelets appeal to engineers as well as to scientists. Image coding, speech processing, coherent state study in physics, are but few of the applications of wavelets.

The Fourier transform of a given signal gives a frequency content of the signal. But it fails to provide information about the time evolution of the frequency content, i.e., how the frequency contents of the given signal change with time. This time-frequency localization is achieved by wavelet transform. The wavelet transform of signal evolving in time depends on two variables, scale (a) and time (b).

$$(W_\psi f)(a,b) = \frac{1}{|a|^{1/2}} \int_{-\infty}^{\infty} f(t)\psi\left(\frac{t-b}{a}\right) dt \tag{2.7}$$

where $\psi(t)$ is the mother wavelet which satisfies the admissibility condition given by

$$C_\psi = 2\pi \int_{-\infty}^{+\infty} \frac{|\hat{\psi}(\xi)|^2}{|\xi|} d\xi < \infty \tag{2.8}$$

where $\hat{\psi}(\xi)$ is the Fourier transform of $\psi(t)$. This requires $\int_{-\infty}^{+\infty} \psi(t)dt = 0$. When the wavelet satisfies the above condition, the inverse wavelet transform exists and is given by

$$f(t) = \frac{1}{C_\psi} \int_{-\infty}^{\infty} \int_{-\infty}^{\infty} (W_\psi f)(a,b)\, \psi\left(\frac{t-b}{a}\right) \frac{1}{|a|^{1/2}} da\, db \tag{2.9}$$

This scaling in the wavelet transform helps to zoom into the short lived high frequency signal or zoom out to the lengthy low frequency signal, by varying the width of the support of the function $\psi(t)$ [5, 6]. This property of the wavelet transform distinguishes it from other time frequency analysis techniques such as window Fourier transform. The discrete wavelet transform is obtained by sampling the parameters a and b in the following manner, $a = a_0^m$ and $b = nb_0a_0^m$ with $a_0 > 1$ and $b_0 > 0$

In general the continuous and discrete wavelet transform are redundant representation of a given signal. For some very special choice of ψ, a_0 and b_0, the redundancy in the wavelet representation is removed. It has been proved that if we choose $a_0 = 2$ *and* $b_0 = 1$ then $\{\psi_{mn} : m,n \in \mathcal{Z}\}$ constitute an orthonormal basis of $L^2(\mathcal{R})$ ([5]). This removes the redundancy in the representation. In this case we define $\psi_{mn} = 2^{-m/2}\psi(2^{-m}t - n)$. The wavelet transform pair is now given by,

$$f_{mn} = \int f(t)\psi_{mn}(t)\, dt \tag{2.10}$$

and

$$f(t) = \sum_{m,n} f_{mn}\psi_{mn}(t) \tag{2.11}$$

It has been shown by Mallat[14] that orthonormal wavelets are closely related to Multiresolution Analysis (MRA). A sequence of vector spaces $\{V_j : j \in \mathcal{Z}\}$ is said to be a Multiresolution Analysis of $L^2(\mathcal{R})$ if they satisfy the following properties and the theorems stated below.

i. $\ldots \subset V_2 \subset V_1 \subset V_0 \subset V_{-1} \subset V_{-2} \subset \ldots$

ii. $\bigcup_{j\in\mathcal{Z}} V_j = L^2(\mathcal{R})$

iii. $\bigcap_{j\in\mathcal{Z}} V_j = \{0\}$

iv. if $f(t) \in V_j$ then $f(2^j t) \in V_0$

v. if $f(t) \in V_0$ then $f(t-k) \in V_0$ for $k \in \mathcal{Z}$

Theorem : 1 For a given multiresolution analysis of $L^2(\mathcal{R})$, there exists a function $\phi(t)$ such that $\{\phi_{mn}(t) : n \in \mathcal{Z}\}$ forms a basis of V_m, where $\phi_{mn}(t) = 2^{-m/2}\phi(2^{-m}t - n)$. The function $\phi(t)$ is unique and is the called scaling function.

Theorem : 2 Associated with each MRA, is a unique orthonormal wavelet $\psi(t)$.

MRA, besides providing a framework for understanding of wavelet bases, has led to the development of fast algorithms to compute Discrete wavelet transforms and Inverse discrete wavelet transforms by indicating the relation between the wavelet transform and subband techniques[5]. This relation between discrete wavelet transform(DWT) and the subband technique also establishes another important property of the DWT, namely, the DWT of a signal divides the frequency spectrum of the given signal into frequency bands with constant relative bandwidth. More specifically, the DWT at a scale 2^m, gives the frequency content of the signal in the range of $\frac{1}{2^{m+1}T} < f < \frac{1}{2^m T}$, T being the sampling interval. Hence the energy of the DWT coefficients at a scale 2^m gives an estimate of the signal energy in that frequency band.

Figures 2.2 and 2.3 show the subband implementation scheme to compute the DWT and the IDWT . In the figure 2.2, $\tilde{h}(n) = h(-n)$ and $\tilde{g}(n) = g(-n)$, where h(n) and g(n) are respectively the discrete low pass and the high pass filters associated with $\psi(t)$ and

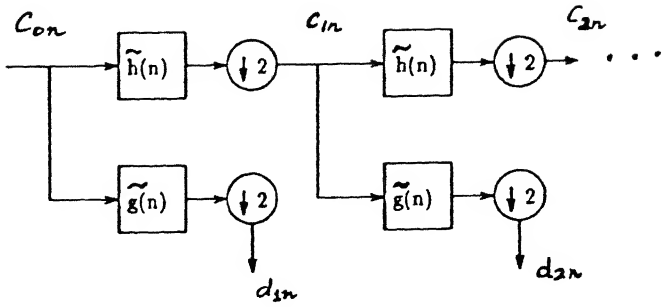

Figure 2.2: *Computing wavelet coefficients through subband technique*

$\phi(t)$ given by equations 2.12 and 2.13.

$$h(n) = \frac{1}{\sqrt{2}} \int \phi(t/2)\phi(t-n)\,dt \tag{2.12}$$

$$g(n) = \frac{1}{\sqrt{2}} \int \psi(t/2)\phi(t-n)\,dt \tag{2.13}$$

for $n \in \mathcal{Z}$ [5, 14, 15].

The sequence c_{0n}, in the figure 2.2 and 2.3 is the inner product of $f(t)$ with $\phi_{0n}(t)$ at the fine resolution level 2^0. $\{d_{mn} : m = 1, 2 \ldots, M\}$ represent the wavelet coefficients which are the detailed signals at the given resolution level 2^{-m} (scale 2^m). They represent the difference in information between the blurred signals $c_{(m-1)n}$ at resolution $2^{-(m-1)}$ and c_{mn} at resolution 2^{-m}. Hence they are also called as difference signals. Similarly c_{mn} represent the blurred signal at the given resolution level 2^{-m}, which represent the blurred version of the original discrete signal c_{0n}.

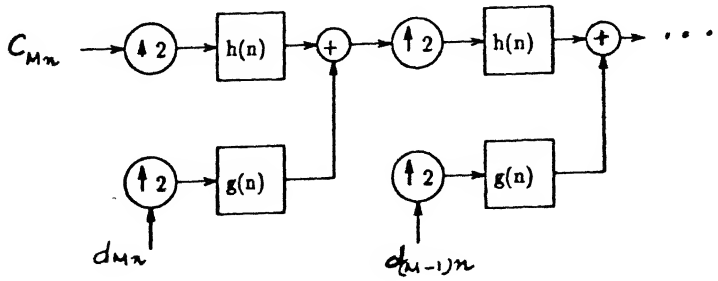

Figure 2.3: *Inverse wavelet transform through subband techniques*

2.3 Detection Theory

Consider the following detection problem,

$$\begin{aligned} y &= x + w \quad : \text{H1} \\ y &= w \quad\quad : \text{H0} \end{aligned}$$

where w is the standard normal random variable $N(0, \sigma^2)$ and x is a deterministic signal with values in the range [R1,R2], $R1 < R2$. The problem of determining whether y is due to signal (hypothesis H1) or due only to noise (hypothesis H0) is optimally solved through the likelihood ratio test when R1,R2 are both positive[7]. In this case this is an Uniformly Most Powerful test (UMP). The likelihood ratio test is given by,

$$y \underset{H0}{\overset{H1}{\gtrless}} \gamma$$

where γ is the threshold. The threshold can be fixed, for e.g., by specifying the desired probability of false alarm.

If $R1 < 0$ and $R2 > 0$, it can be shown that the UMP doesnot exist([7]). Then we resort to some suboptimal tests such as the generalized likelihood ratio test (GLRT), given by

$$|y| \underset{H0}{\overset{H1}{\gtrless}} \gamma \tag{2.14}$$

The equation 2.14 will be used in our work.

Chapter 3

Wavelet Preprocessing of Noisy Projections

In this chapter we discuss the problem of noise suppression and propose a possible solution through time variant filtering, within the following framework.

- The noise is Additive White Gaussian.
- Signals considered are *spacelimited and resolution limited* . Essentially bandlimited signals which are represented by finite number of samples belong to this class of signals [10, 11].
- *No a priori* knowledge about the nature of input image and its projections is assumed.

3.1 Time variant filtering

The fine scale wavelet transform coefficients (those corresponding to smaller m in 2^m) represent the localized high frequency contents of the signal. Hence, setting all the fine scale coefficients to zero will amount to low pass filtering the original signal. This process, which is equivalent to time invariant filtering, reduces noise, at the expense of edge information present in those high frequency components. If we choose to set only those wavelet coefficients whose absolute values are less than a particular threshold to zero, then we can still preserve the edges while reducing the effect of noise [9] . Such selective zeroing of the wavelet coefficients, which is equivalent to time variant filtering, is justified by the GLRT, discussed in section 2.3.

Let $y(s_i,\theta_j), g(s_i,\theta_j)$ and $w(s_i,\theta_j)$ represent the discrete forms of the noisy projections $[y(s,\theta)]$, noiseless projections $[g(s,\theta)]$ and the white noise $[w(s,\theta)]$. Here, $s_i \in \mathcal{N} = \{0, D, \ldots, (N-1)D\}$ and $\theta_j \in \Theta = \{0, \pi/K, 2\pi/K, \ldots, (K-1)\pi/K\}$, where N and K are the number of samples in 's' and θ respectively and D is the sampling interval along 's'. Hence, the discrete noisy projections can be written as, $y(s_i,\theta_j) = g(s_i,\theta_j) + w(s_i,\theta_j)$ The problem is to estimate g(.) from y(.). We can represent the signal y(.) in terms of its orthogonal components, along some convenient orthonormal basis (We use orthonormal wavelets for this purpose).

Let $y^{\theta}_{mn}, g^{\theta}_{mn}$ and w^{θ}_{mn} be the discrete wavelet transform of $y(s_i,\theta_j), g(s_i,\theta_j)$ and $w(s_i,\theta_j)$ respectively. Because of the orthonormal representation w^{θ}_{mn} are independent Gaussian random variables. From the linearity property of the wavelet transform it follows that,

$$y^{\theta}_{mn} = g^{\theta}_{mn} + w^{\theta}_{mn}$$

For notational convenience we have used $\theta \in \Theta$ in place of θ_j.

The data available for the detection problem now is $\{y^{\theta}_{mn} : m \in \mathcal{M}, n \in \mathcal{N}_m, \theta \in \Theta\}$ where $\mathcal{M} = \{1, 2, \ldots, M\}$ is the set of available distinct difference levels, $\mathcal{N}_m = \{0, 1, \ldots, N_m - 1\}$ and N_m is the number of samples at each difference level m. We would like to determine which of these available detailed coefficients are due to signal and noise respectively. The suboptimal test given by equation 2.14 can be used to determine this, i.e., if $|y^{\theta}_{mn}| > \gamma(m)$ then it is due to signal, otherwise it is due to noise. The result of this hypothesis testing is the detected coefficient set $\breve{g}^{\theta}_{mn}$, which are given by,

$$\breve{g}^{\theta}_{mn} = \begin{cases} y^{\theta}_{mn} & \text{if } |y^{\theta}_{mn}| > \gamma(m) \\ 0 & \text{if } |y^{\theta}_{mn}| < \gamma(m) \end{cases} \qquad (3.1)$$

This is precisely the time variant filter which we discussed earlier. The detected coefficients $\breve{g}^{\theta}_{mn}$ are used to reconstruct the preprocessed signal $\breve{g}(s_i,\theta_j)$ through inverse wavelet transform. This is then used to obtain the noise suppressed image through inverse Radon Transform.

3.2 Deciding the threshold

We now turn our attention to the problem of fixing the threshold. In this work, we choose a threshold based on energy criterion [11]. As noted earlier, the wavelet transform, decomposes a signal into a group of detailed signals, each corresponding to a particular frequency band of constant relative bandwidth. The energy at a specific detailed level gives the estimate of the signal's energy in that frequency band. We can estimate the information signal energy from the observed signal energy and the noise variance.

Referring to figure 2.2 and 2.3, we note that with subband implementation scheme the detailed signal at the scale 2^m is obtained by passing the original discrete signal through m-1 stages of lowpass filters [h(n)] and a single stage of highpass filter [g(n)]. The variance of the Gaussian random variable at the output, for $N(0,\sigma^2)$ as input, is given by [8],

$$\sigma_m^2 = \sigma^2 \left[\sum_n (h(n))^2\right]^{m-1} \left[\sum_n (g(n))^2\right] \tag{3.2}$$

Therefore the noise energy at this difference level is

$$P_{w_m} = N_m \sigma_m^2 \approx 2^{-m} N \sigma_m^2 \tag{3.3}$$

Also the observed signal energy,p_{y_m}, at the level m (scale 2^m), is given by

$$P_{y_m} = \sum_{n=0}^{N_m} (y_{mn})^2 \tag{3.4}$$

Using equations 3.3 and 3.4 we can estimate the information signal energy, i.e., uncorrupted signal energy $P_{g_m^\theta}$, as

$$P_{g_m^\theta} = P_{y_m} - 2^{-m} N \sigma_m^2 \tag{3.5}$$

This estimate is used to fix the threshold in the equation (3.1). We vary the threshold in such a way that the thresholded signal energy $P_{\breve{g}_m^\theta} = \sum_n (\breve{g}_{mn}^\theta)^2$, approximates the estimated signal energy.

The proposed technique has been tested on computer simulated images and the results are given in chapter 5.

Chapter 4

2-D Wavelet Transform

In this section, we prove that the reconstructed image from the wavelet transform (at a fixed scale) of the the projections is the two dimensional wavelet transform of the original image at that scale.

Proof :

1. The one dimensional wavelet transform of the projection $g(s,\theta)$, at a particular resolution, a,

$$g_a(s,\theta) = \frac{1}{\sqrt{a}} \int g(t,\theta)\psi\left(\frac{t-s}{a}\right) dt$$

can be written as,

$$g_a(s,\theta) = g(s,\theta) \otimes_1 \left[\frac{1}{\sqrt{a}}\psi\left(\frac{-s}{a}\right)\right]$$

From the convolution property of the Radon transform (equation 2.6), we have

$$G_a(x,y) = F(x,y) \otimes_2 \Psi_a(-x,-y) \tag{4.1}$$

where $G_a(x,y)$, $F(x,y)$ and $\Psi_a(-x,-y)$ are the inverse Radon Transforms of $g_a(s,\theta)$, $g(s,\theta)$ and $(1/\sqrt{a})\psi(-s/a)$ respectively; $\otimes_1, \otimes_2$ denote the one dimensional and two dimensional convolution respectively.

2. Consider the function, $\Psi_a(-x,-y)$, which is the inverse Radon transform of $\frac{1}{\sqrt{a}}\psi(-\frac{s}{a})$, i.e.,

$$\Psi_a(-x,-y) = \frac{1}{\sqrt{a}} \int_0^{\pi} \int_{-\infty}^{\infty} \psi\left(\frac{-s}{a}\right) p(x\cos\theta + y\sin\theta - s)\, ds\, d\theta$$

where p(s) is the ramp filter as defined in section 2.1. Since p(s) is symmetric, we can write,

$$\Psi_a(x,y) = \frac{1}{\sqrt{a}} \int_0^{\pi} \int_{-\infty}^{\infty} \psi\left(\frac{s}{a}\right) p(x\cos\theta + y\sin\theta - s)\, ds\, d\theta$$

With a change of variable, $s/a = r$, we have,

$$\begin{aligned} \Psi_a(x,y) &= \frac{a}{\sqrt{a}} \int_0^{\pi} \int_{-\infty}^{\infty} \psi(r) p(x\cos\theta + y\sin\theta - ar)\, dr\, d\theta \\ &= \frac{a}{\sqrt{a}} \int_0^{\pi} \int_{-\infty}^{\infty} \psi(r) p\left[a\left(\frac{x}{a}\cos\theta + \frac{y}{a}\sin\theta - r\right)\right] dr\, d\theta \end{aligned} \tag{4.2}$$

We know that $p(s) \overset{F.T}{\longleftrightarrow} |\xi|/(2\pi)$. Now,

$$p(as) \overset{F.T}{\longrightarrow} \frac{1}{a}\frac{|\xi/a|}{2\pi} = \frac{1}{a^2}\frac{|\xi|}{2\pi} \overset{I.F.T}{\longrightarrow} \frac{1}{a^2} p(s)$$

where F.T. and I.F.T. represent Fourier transform and Inverse Fourier transform respectively. Hence,

$$p(as) = \frac{1}{a^2} p(s) \tag{4.3}$$

Using equation 4.2 and 4.3

$$\begin{aligned} \Psi_a(x,y) &= \frac{1}{a\sqrt{a}} \int_0^{\pi} \int_{-\infty}^{\infty} \psi(r) p\left(\frac{x}{a}\cos\theta + \frac{y}{a}\sin\theta - r\right) dr\, d\theta \\ &= \frac{1}{a\sqrt{a}} \Psi\left(\frac{x}{a}, \frac{y}{a}\right) \end{aligned}$$

where

$$\Psi(x,y) = \int_0^{\pi} \int_{-\infty}^{\infty} \psi(r) p(x\cos\theta + y\sin\theta - r)\, dr\, d\theta$$

Thus we have shown that,

$$\Psi_a(x,y) = \frac{1}{a\sqrt{a}} \Psi\left(\frac{x}{a}, \frac{y}{a}\right) \tag{4.4}$$

that is, $\Psi_a(x,y)$ is the scaled version of the 2D signal $\Psi(x,y)$. Hence the convolution in the equation 4.1 is the convolution with the same signal which is scaled in both x and y by an amount a.

3. Now we show that $\Psi(x,y)$ satisfies the admissibility condition,i.e.,

$$C_{\Psi} \triangleq (2\pi)^2 \int_{-\infty}^{\infty} \frac{|\hat{\Psi}(a\xi_1, a\xi_2)|^2}{|a|}\, da < \infty \tag{4.5}$$

Now,

$$\hat{\Psi}(a\xi_1, a\xi_2) \xrightarrow{2dIFT} \frac{1}{|a|^2}\Psi(\frac{x}{a}, \frac{y}{a}) \xrightarrow{RT} \frac{1}{|a|}\psi(\frac{s}{a}) \xrightarrow{1dFT} \hat{\psi}(a\xi)$$

where 2dIFT, RT and 1dFT represent the 2-D inverse Fourier transform, Radon Transform and 1-D Fourier transform respectively. But from Projection slice theorem, we know that the 1-D Fourier transform of Radon transform of a function is the same as the 2-D Fourier transform of the function. Therefore,

$$\hat{\Psi}(a\xi_1, a\xi_2) = \hat{\psi}(a\xi) \tag{4.6}$$

From 4.5 and 4.6, we have,

$$\begin{aligned} C_\Psi &= (2\pi)^2 \int_{-\infty}^{\infty} \frac{\hat{\psi}(a\xi)}{|a|}\, da \\ &= 2\pi C_\psi \end{aligned}$$

But, from equation 2.8, $C_\psi < \infty$ because the one dimensional wavelet $\psi(x)$ is admissible. Therefore $C_\Psi < \infty$ and hence the two dimensional wavelet, $\Psi(x, y)$ is admissible. Here we made use of Fourier Slice Theorem.

We summarise our result below,

- Compute the discrete wavelet transform (the detailed coefficients d^θ_{mn} of the projections) and the blurred signal c^θ_{Mn} through subband technique, where $m \in \mathcal{M}$ and $n \in \mathcal{N}_m$.
- Reconstruct the image at a particular resolution from the wavelet transform of the projection.

We give the schematic of the given algorithm in figure 4.1. This property is demonstrated using computer calculated projections of simulated images and the results are given in chapter 5.

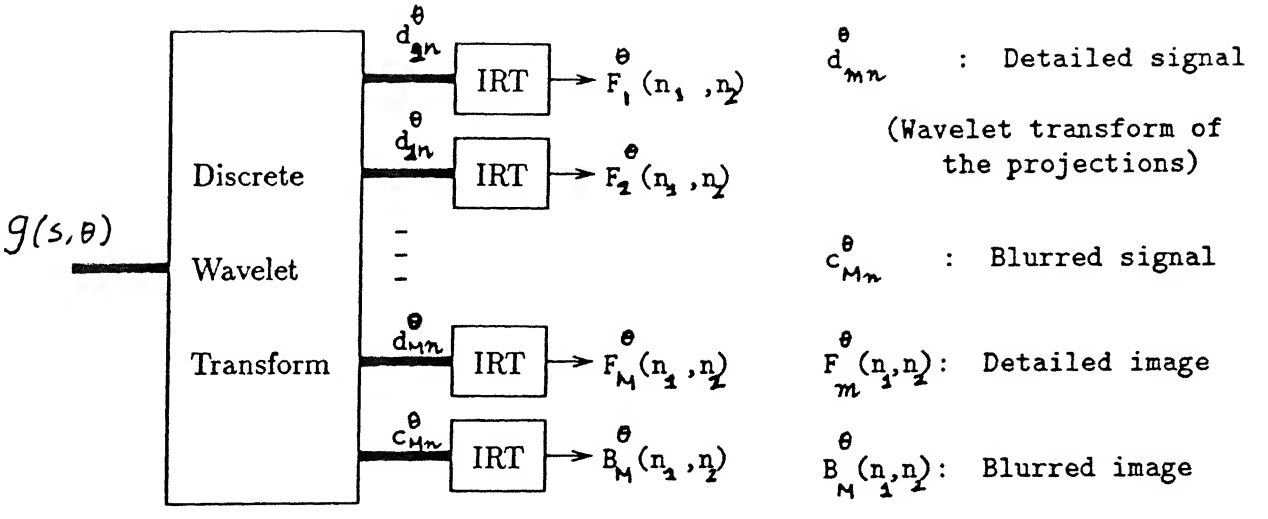

Figure 4.1: *Schematic of the given algorithm*

Chapter 5

Simulation Results

In this chapter, the results of the chapters 3 and 4 have been verified through simulation. We first present the simulations results of wavelet preprocessing of noisy projections. Then we present the results of the simulations of 2D wavelet transform. We have used Daubechies's compactly supported wavelet of length 16.

5.1 Wavelet Preprocessing

We use two test images to demonstrate the noise suppressing and edge preserving properties of the algorithm presented in chapter 3. We add white Gaussian noise to the projections of the test image. The thresholding technique(equation 3.1) is used to process the noisy projections. These processed projections are then used to reconstruct the image to give the noise suppressed image.

The details of the test image and the simulation results are given below.

- a.

$$f(x,y) = \begin{cases} 1 & \text{if } |x| < 0.5 \text{ and } |y| < 0.5 \\ 0 & \text{otherwise} \end{cases}$$

The function is defined over the square $-1 \leq x, y \leq 1$. The Radon transform, $g(s,\theta)$, of this function, for $-\sqrt{2} \leq s \leq \sqrt{2}$ and $0 \leq \theta \leq \pi/4$ is given by,

$$g(s,\theta) = \begin{cases} \frac{s+0.5\cos\theta+0.5\sin\theta}{\sin\theta\cos\theta} & -0.5\cos\theta - 0.5\sin\theta \leq s \leq -0.5\cos\theta + 0.5\sin\theta \\ \frac{1}{\cos\theta} & -0.5\cos\theta + 0.5\sin\theta \leq s \leq 0.5\cos\theta - 0.5\sin\theta \\ \frac{-s+0.5\cos\theta+0.5\sin\theta}{\sin\theta\cos\theta} & 0.5\cos\theta - 0.5\sin\theta \leq s \leq 0.5\cos\theta + 0.5\sin\theta \end{cases}$$

Symmetry of the figure is used to obtain the value of $g(s,\theta)$ for $\pi/4 \leq \theta < \pi$.

We have used samples of $g(s,\theta)$ with 127 samples in variable s (number of rays per projection) and 40 samples in variable θ (number of projections) to reconstruct the test image on a grid of 51×51. Reconstruction from noiseless projections, $g(s,\theta)$, is shown in figure 5.3. We add white Gaussian noise with zero mean and variance 0.0004. Reconstruction from these noisy projections is shown in figure figure 5.4. The noisy projections are then processed using the thresholding technique(equation 3.1). The reconstruction from the processed projections is shown in figure 5.5. Reconstruction from noisy projection was also done using the space invariant filter(equation 2.4) technique. To compare the reconstruction using the thresholding technique with the space invariant filtering technique, we plot the cross section through each image along the line x=0 in figure 5.7. From figure 5.7, we observe that the reconstructed image after preprocessing closely approximates the noiseless reconstructed image at the edges. However, we observe from figure 5.8, this is not the case for the reconstructed image using space invariant filtering technique. We also note from figure 5.7 that the noise performance of the thresholding technique is as good as the space invariant filtering technique.

- b. Shepp-Logan's Head Phantom :

  We now repeat the above process on Shepp-Logan phantom [13]. This phantom, which is frequently used in medical imaging, is supposed to be a cross sectional view of the human head with denser areas indicating tumors and the less dense areas indicating the spinal fluid [9]. Figure 5.1 shows this phantom. We have used samples of the Radon transform $g(s,\theta)$ with 255 samples in the variable s and 100 samples in variable θ to reconstruct the test phantom on a grid of 99×99. Reconstruction from noiseless projection is shown in figure 5.9. We then add white Gaussian noise with zero mean and variance 1×10^{-6}. Reconstruction from these noisy projections is shown in figure 5.10. The noisy projections are processed using the thresholding technique. Image reconstructed from these processed projections is shown in figure 5.11. Figures 5.13 to 5.14 show the cross sections of these reconstructed images along the lines x=0 and y=0.

5.2 2D wavelet transform

The results of chapter 4 are demonstrated on a test image. The test image used in this case is shown in figure 5.2. Reconstruction is done on a grid of 79×79 from 50 projections with 255 rays per projections. The reconstruction from noiseless projections is shown in figure 5.15. We consider the original discrete projections to be at resolution level 2^0. Using subband technique (refer figure 2.2), detailed signals at resolution levels 2^{-1} and 2^{-2} (i.e. the wavelet transform at the scale a=2 and 2^2) of the projections are calculated along with the blurred signal at 2^{-2}. Reconstructed images from the detailed signals and the blurred signal of the projections at these resolution levels are shown in figures 5.16-5.18. We note that the image reconstructed from the detailed signal give the local high frequency information i.e., the edge information, of the original image.

We add white Gaussian noise to these projections with variance 0.0001. After thresholding is done in the wavelet transform domain, instead of taking inverse wavelet transform to get the processed projections, we reconstruct the images as mentioned before. This results in the noise suppressed 2 dimensional wavelet transform of the original image from noisy projections. The image thus reconstructed from the noise supressed detailed signal, at resolution 2^{-1}, of the projections is shown in the figure 5.19. The wavelet transform at this scale represent the high frequency part of the projections. Thus here noise dominates the signal. In figure 5.19, we observe that the the thresholding technique has essentially removed this noise.

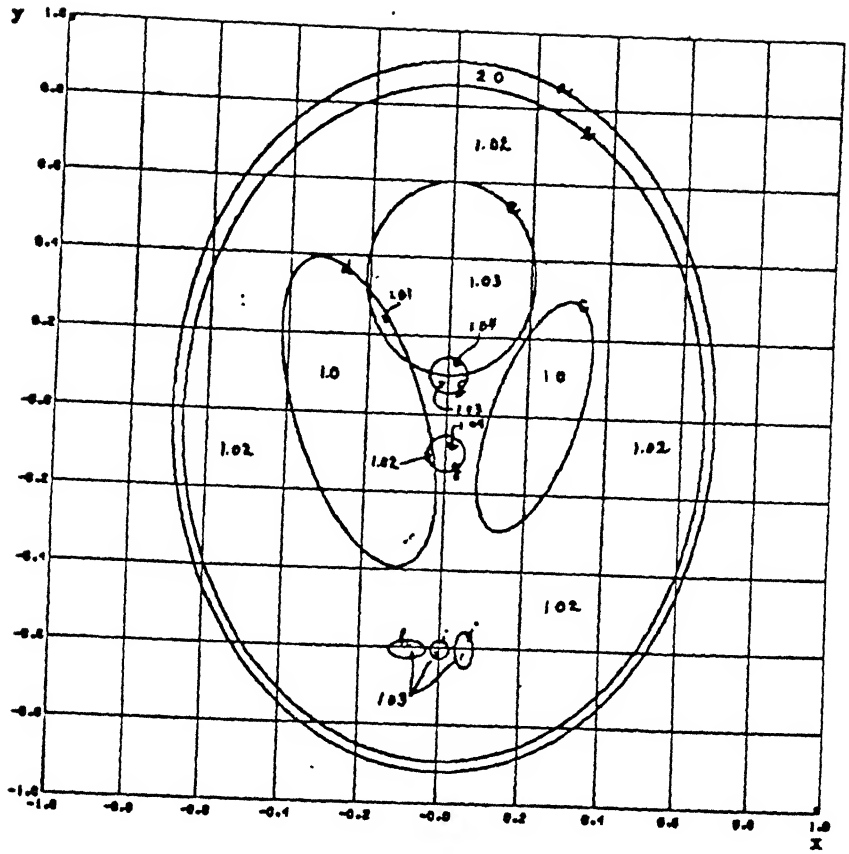

Figure 5.1: *Shepp-Logan Phantom*

Ellipse	$\bar{x}$	$\bar{y}$	Major Axis	Minor Axis	Inclination	Density $f_i(x,y)$
a	0.00	0.0000	0.6900	0.9200	0.00	1.00
b	0.00	−0.0184	0.6624	0.8740	0.00	−0.98
c	0.22	0.0000	0.1100	0.3100	−18.00	−0.02
d	−0.22	0.0000	0.1600	0.4100	18.00	−0.02
e	0.00	0.3500	0.2100	0.2500	0.00	0.01
f	0.00	0.1000	0.0460	0.0460	0.00	0.01
g	0.00	−0.1000	0.0460	0.0460	0.00	0.01
h	−0.08	−0.6050	0.0460	0.0230	0.00	0.01
i	0.00	−0.6050	0.0230	0.0230	0.00	0.01
j	0.00	−0.6060	0.0230	0.0460	0.00	0.01

Table 1: The parameters of the ellipses in Shepp-Logan's head phantom. $(\bar{x},\bar{y})$, represents the centre of the ellipse.

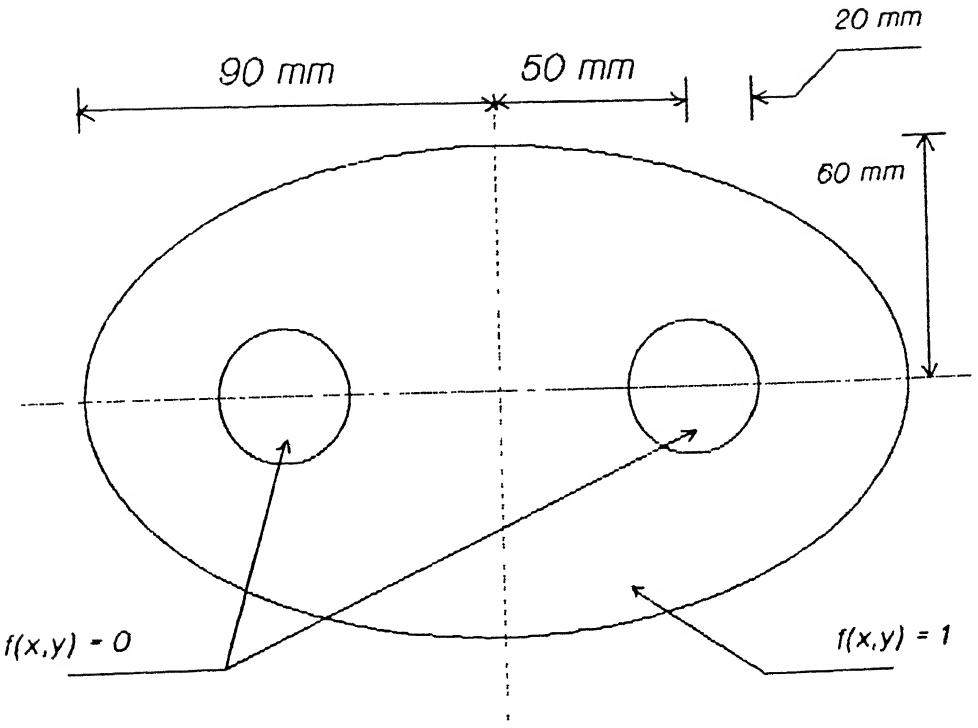

Figure 5.2: *Test Image (Elipse and Circle)*

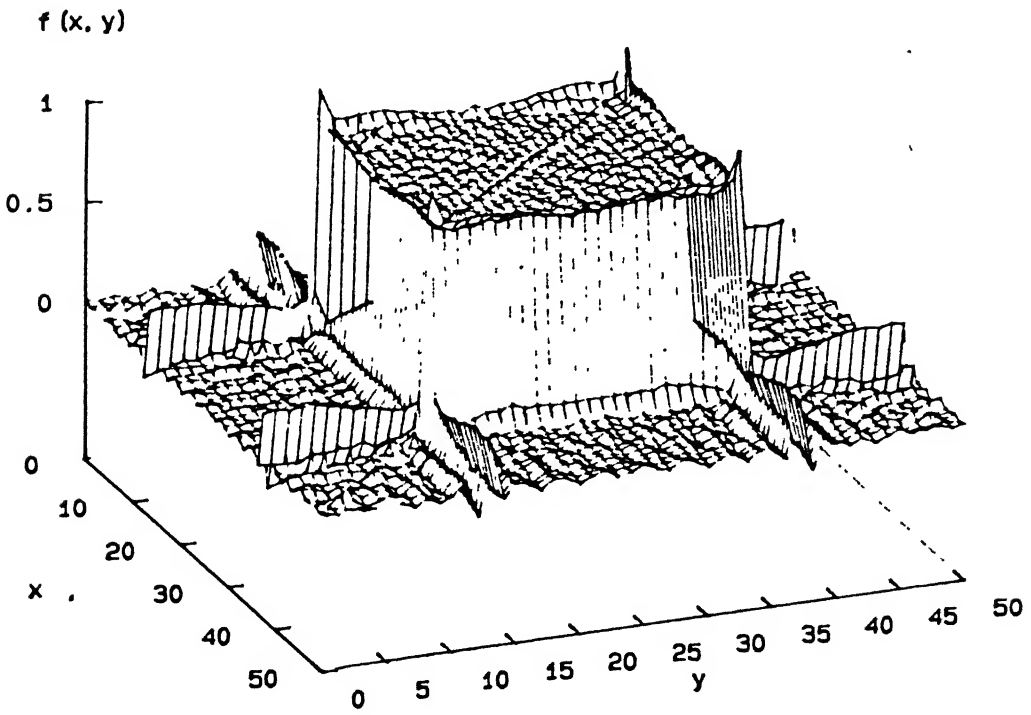

Figure 5.3: *Reconstruction of Square from Noiseless Projections*

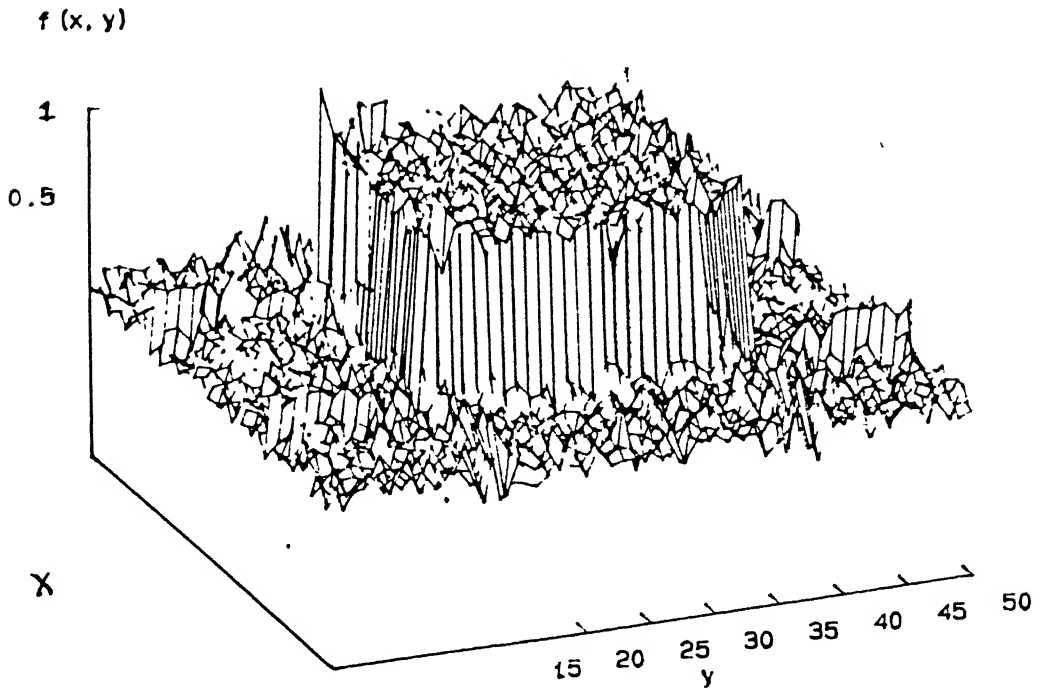

Figure 5.4: *Reconstruction from Noisy Projections (Variance 0.0004)*

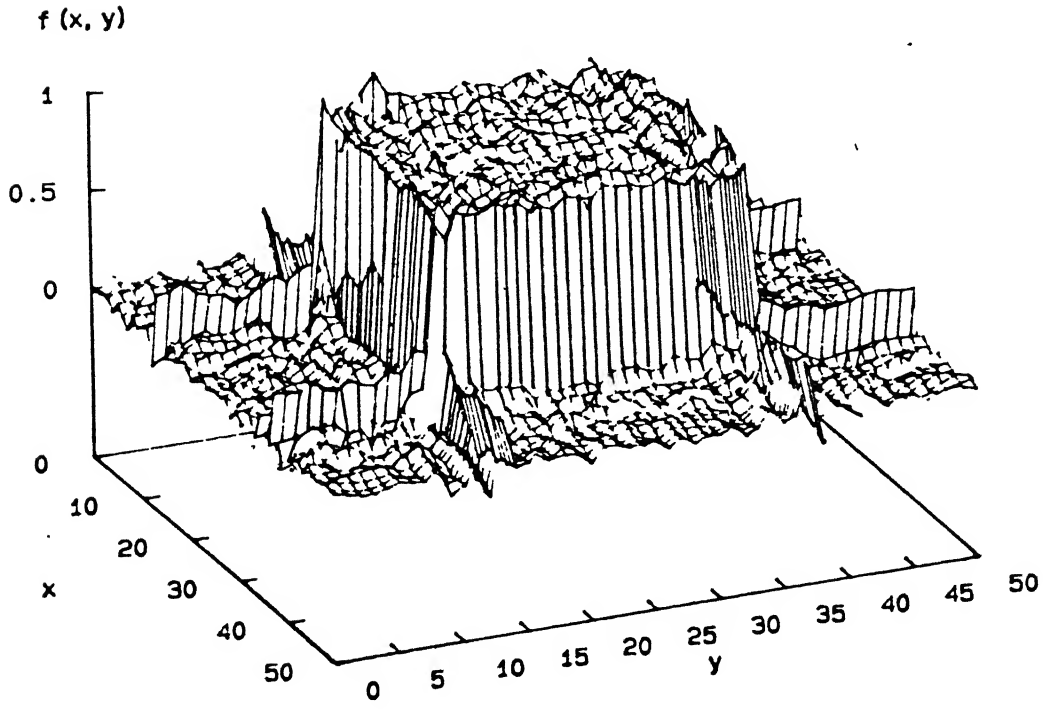

Figure 5.5: *Reconstruction from Preprocessed Projections*

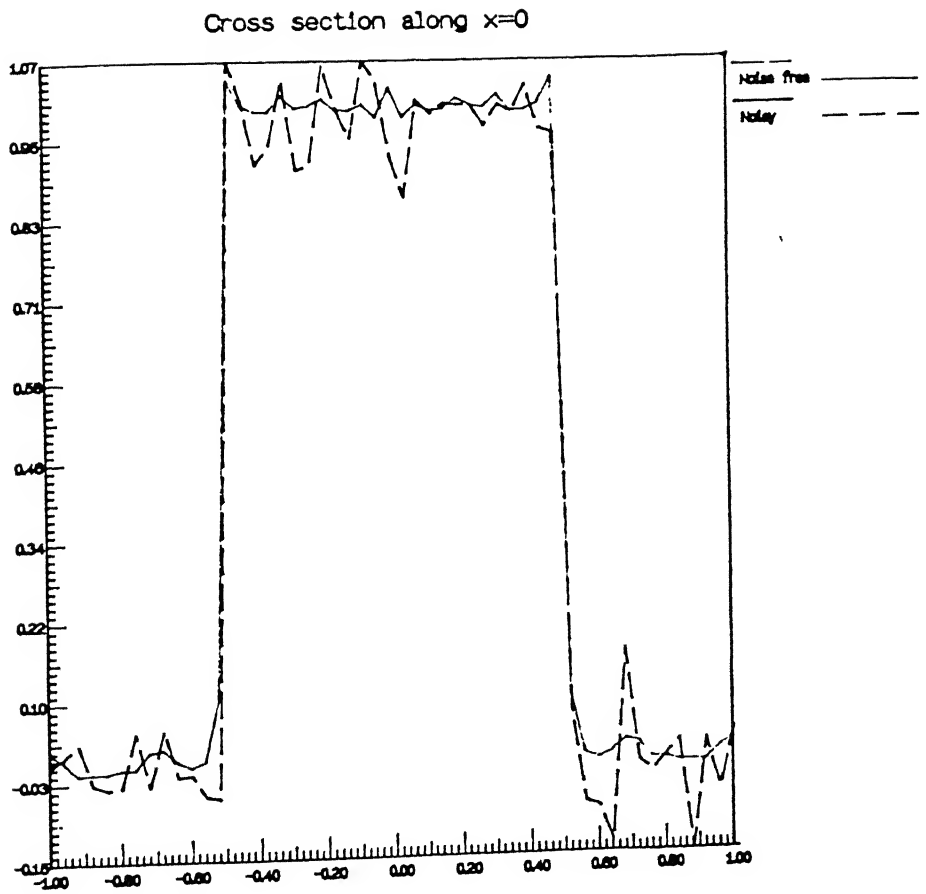

Figure 5.6: *Cross section along x=0 of image reconstructed from noisy projections*

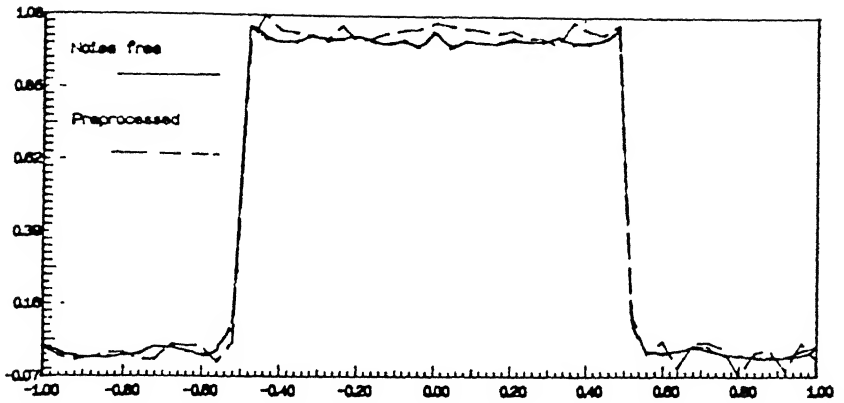

Figure 5.7: *Cross section along x=0 of image reconstructed from wavelet preprocessed projections*

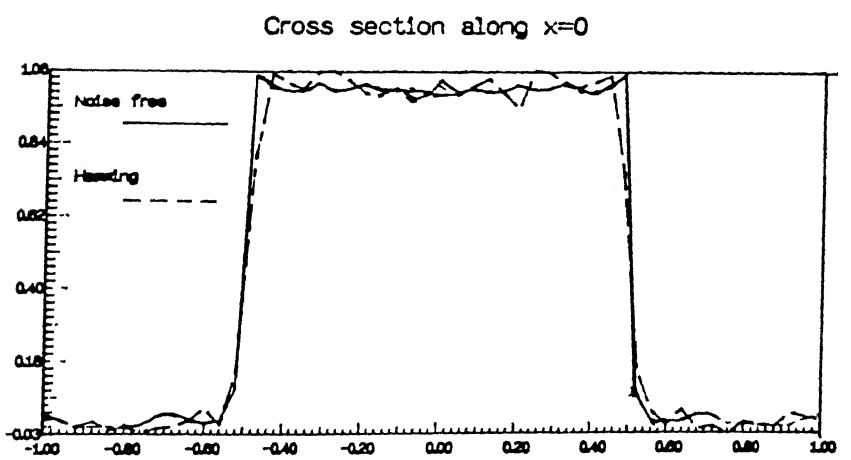

Figure 5.8: *Cross section along x=0 of image reconstructed from space invariant filtered projections*

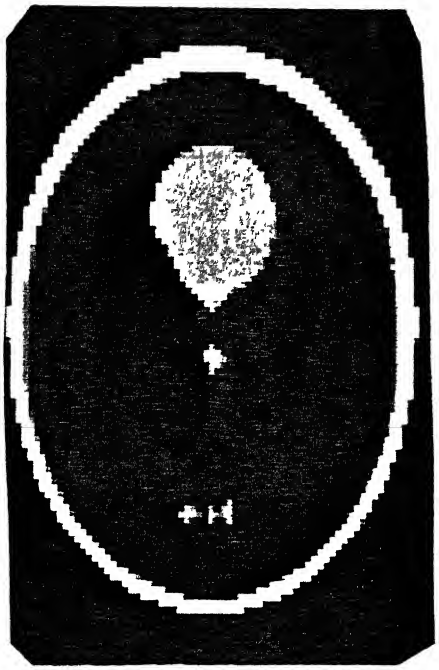

Figure 5.9: *Reconstruction from Noiseless projections*

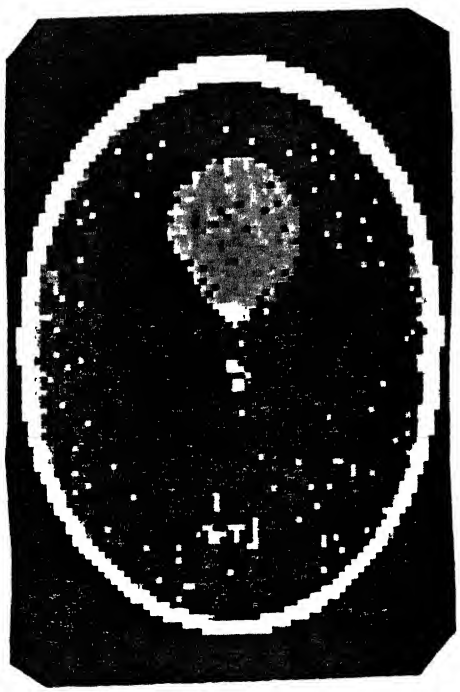

Figure 5.10: *Reconstruction from Noisy projections (Noise Variance* 1×10^{-6}*)*

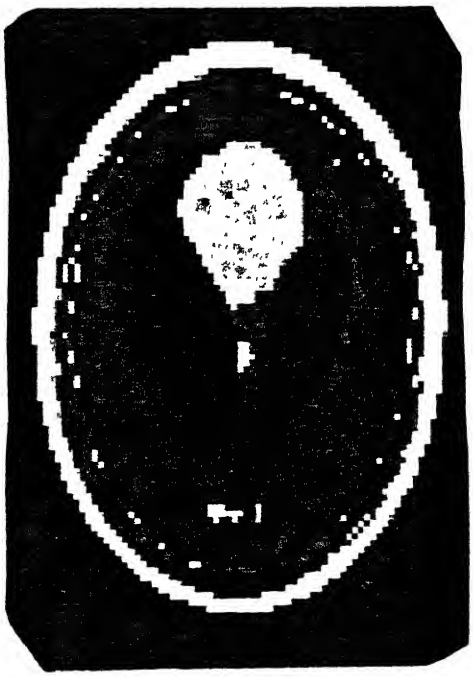

Figure 5.11: *Reconstruction from Preprocessed projections (Noise Variance* 1×10^{-6}*)*

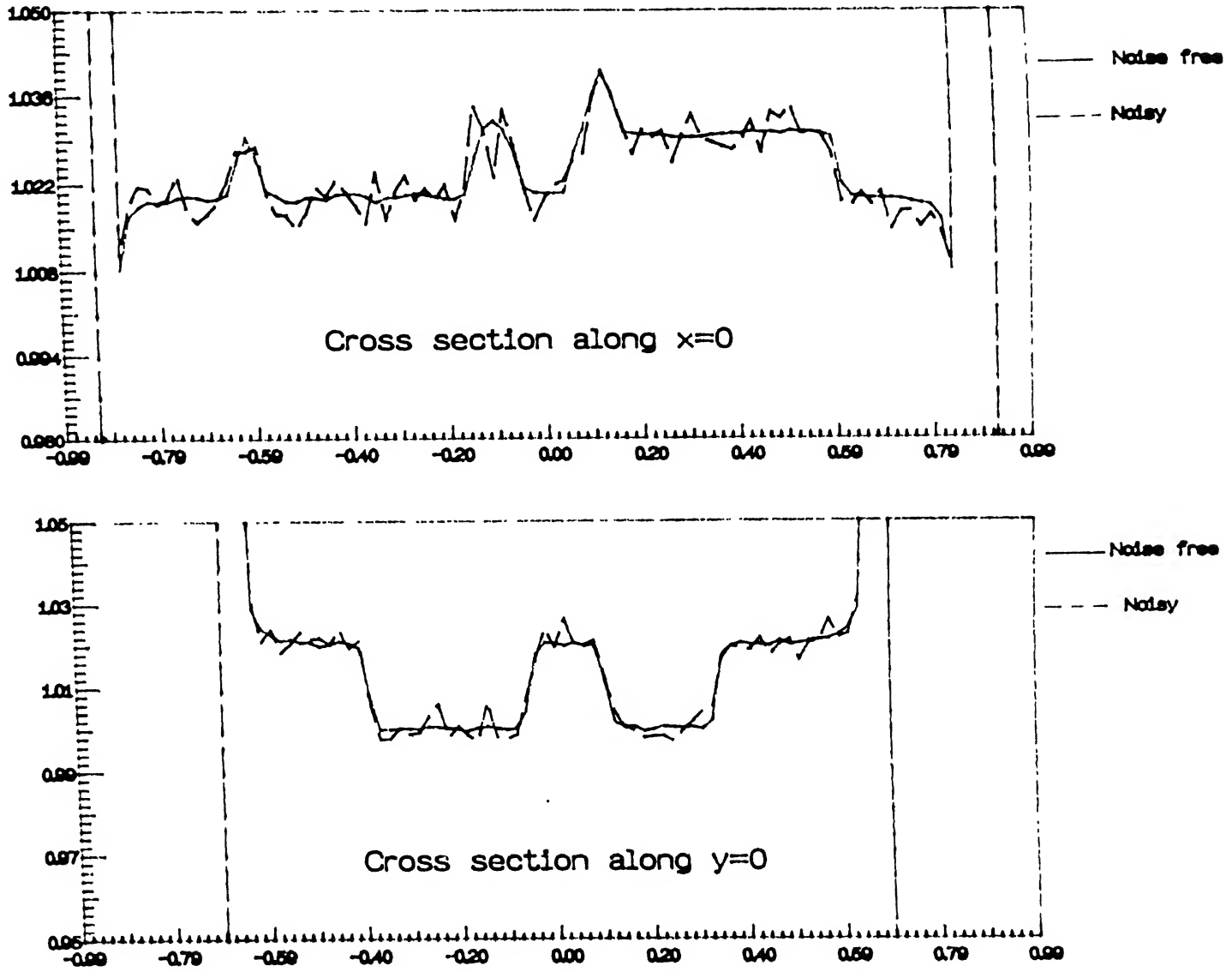

Figure 5.12: *Cross section of phantom reconstructed from Noisy projections (Noise Variance* 1×10^{-6}*)*

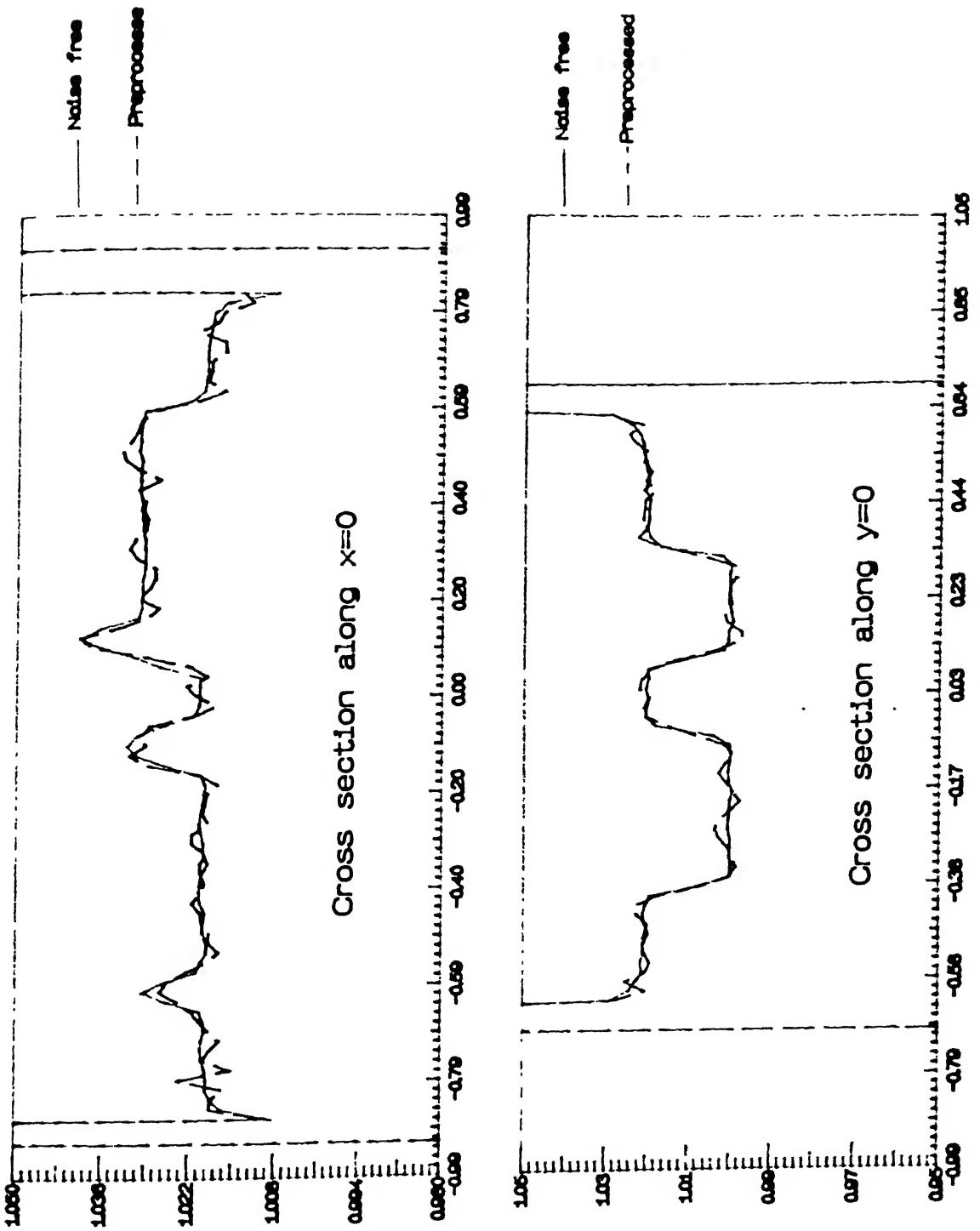

Figure 5.13: *Cross section of phantom reconstructed from Preprocessed projections (Noise Variance* 1×10^{-6})

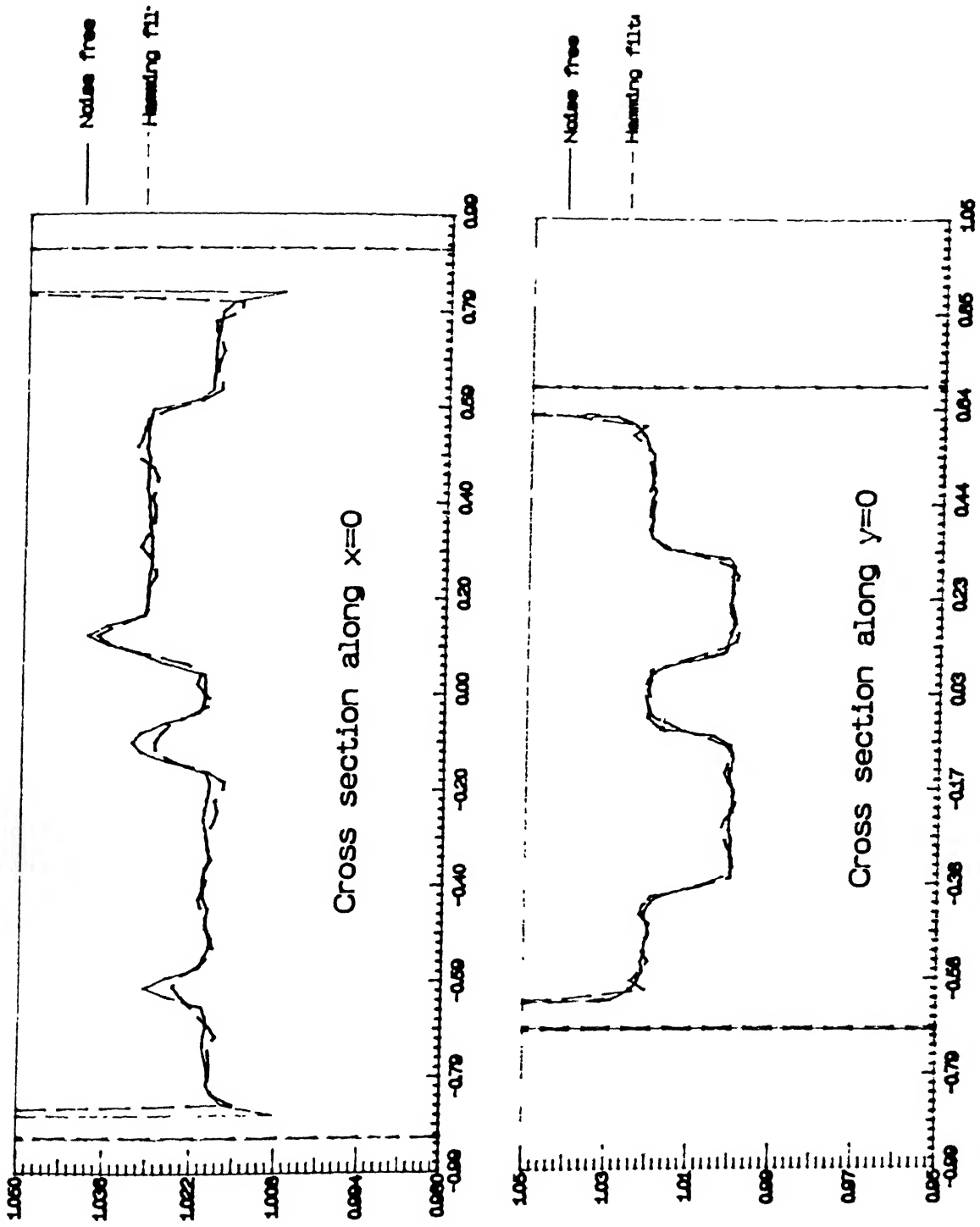

Figure 5.14: *Cross section of phantom reconstructed from space invariant filtered projections (Noise Variance* 1×10^{-6}*)*

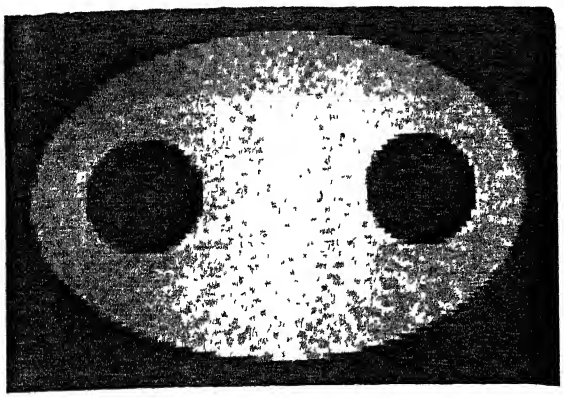

Figure 5.15: *Reconstruction from Noiseless projections*

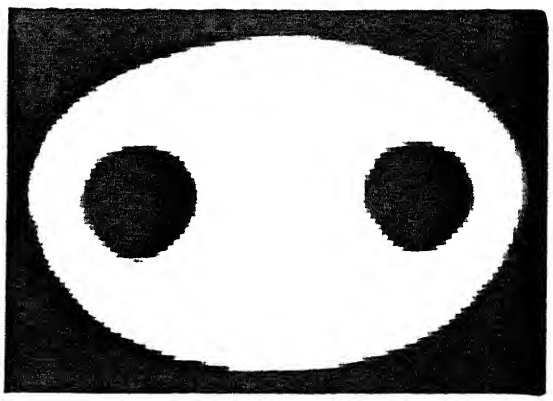

Figure 5.16: *Blurred image at resolution* 2^{-2}

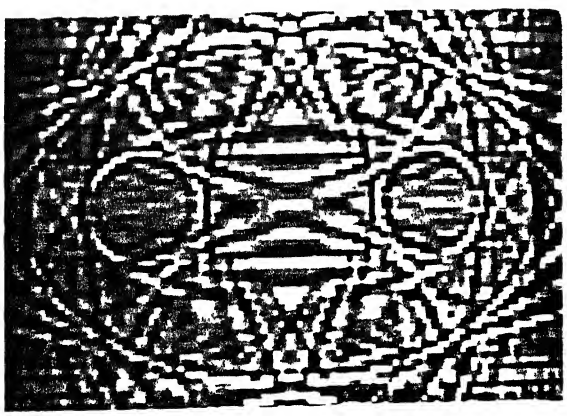

Figure 5.17: *Detailed image at resolution* 2^{-1}

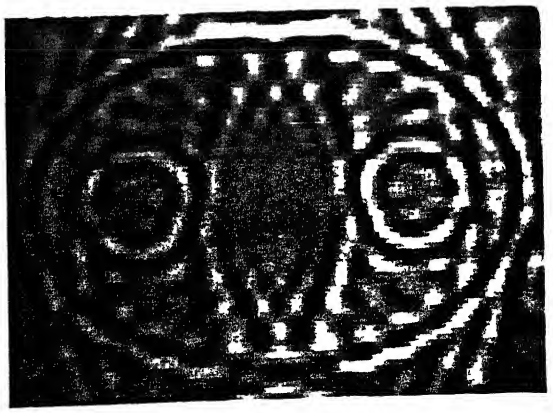

Figure 5.18: *Detailed image at resolution* 2^{-2}

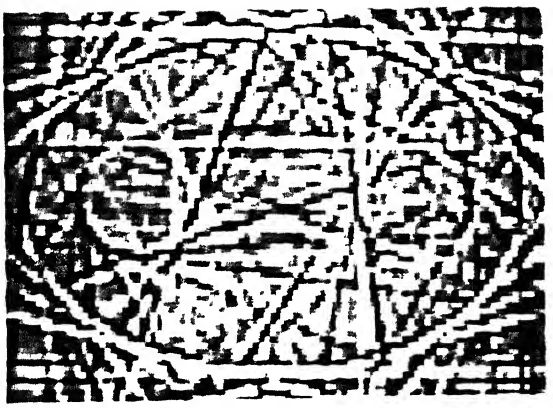

Figure 5.19: *Noise suppressed Detailed image at resolution* 2^{-1} *(Noise variance* 4×10^{-4}*)*

Chapter 6

Scope for Future Work

6.1 Reconstruction of 2D image from its Wavelet transform

In chapter 4, we outlined a method to obtain the two dimensional wavelet transform of an image from its projections. Here we suggest a method to synthesise the image from its available wavelet transform.

From equation 2.12 we have,

$$\begin{aligned} h(n) &= \frac{1}{\sqrt{2}} \int \phi(s/2)\phi(s-n)\, ds \\ &= \left[\frac{1}{\sqrt{2}} \phi(s/2) \otimes_1 \phi(-s) \right]_{s=n} \end{aligned}$$

where $n \in \mathcal{Z}$. Let $h_c(s) = (1/\sqrt{2})\phi(s/2) \otimes_1 \phi(-s)$, i.e., h(n) is the discrete signal obtained by sampling $h_c(s)$ at $s = n; n \in \mathcal{Z}$. Let $H_c(x,y)$ represent the inverse Radon transform (IRT) of $h_c(s)$. From convolution property (equation 2.6) and the scaling property [1],

$$H_c(x,y) = [\frac{1}{2\sqrt{2}} \Phi(\frac{x}{2}, \frac{y}{2})] \otimes_2 \Phi(-x, -y)$$

where $\Phi(x,y)$ is the IRT of $\phi(s)$. Similarly from equation 2.13, we can write,

$$G_c(x,y) = [\frac{1}{2\sqrt{2}} \Psi(\frac{x}{2}, \frac{y}{2})] \otimes_2 \Phi(-x, -y)$$

where $G_c(x,y)$ is the IRT of $g_c(s)$ (which can be sampled at $s = n; n \in \mathcal{Z}$ to give g(n)) and $\Psi(x,y)$ is the IRT of $\psi(s)$ (equation 4.4). Let $H(n_1, n_2)$ and $G(n_1, n_2)$ represent the discrete forms of $H_c(x,y)$ and $G_c(x,y)$ respectively obtained by sampling at $x = n_1, y = n_2; n_1, n_2 \in \mathcal{Z}$.

Let $F_m(n_1, n_2)$ and $B_m(n_1, n_2)$ represent the detailed image and the blurred image at the resolution 2^{-m} obtained by the method suggested in chapter 4. We propose that the blurred image $B_{(m-1)}(n_1, n_2)$ at the next higher resolution viz. $2^{-(m-1)}$ can be obtained as follows,

- Upsample both $F_m(n_1, n_2)$ and $B_m(n_1, n_2)$ by a factor of 2 in both the directions n_1 and n_2.
- Filter the upsampled blurred image with $H(n_1, n_2)$ and the upsampled detailed image with $G(n_1, n_2)$.
- Add the filtered images.

We justify our claim by repeatedly invoking the linearity, convolution and scaling properties of Radon transform. Let c^{θ}_{1n} and d^{θ}_{1n} represent the blurred and detailed signals at the resolution 2^{-1} of the projections of the image $B_0(n_1, n_2)$. These signals are obtained by filtering the projections using h(n) and g(n) respectively and down sampling them by 2. Figure (6.1) shows how to reconstruct the image from c^{θ}_{1n} and d^{θ}_{1n}:

- Making use of linearity property of Radon transform, we can shift the Inverse Radon transform (IRT) block before the adder, noting that the addition will now be two dimensional.
- Making use of convolution property, we can shift the IRT block before the filtering stage. Now the filtering will be two dimensional and it is the filtering of the reconstructed blurred (or detailed) image with the IRT of the function whose discrete representation is h(n) (or g(n) as the case may be).
- Making use of scaling property, we can shift the IRT before the downsampling stage, noting that the down sampling will now be done in two dimensional and will be in both direction n_1 and n_2.

The block diagram after the above modification is as shown in figure 6.2. Since the blurred signal c^{θ}_{1n} can be obtained from c^{θ}_{2n} and d^{θ}_{2n}, applying the same 3 steps, we can show that the IRT of the blurred signal c^{θ}_{1n} and hence the image, $B_0(n_1, n_2)$, can be obtained from the

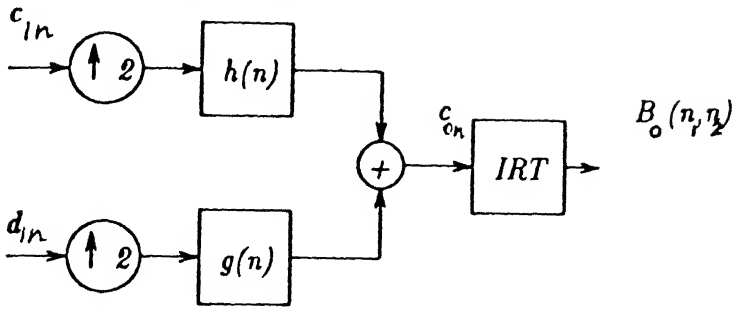

h(n) : Lowpass filter *c : blurred signal*
g(n) : Highpass filter *d : detail signal*
(1-D filters) *(1-D signals)*
B (n ,n) : Blurred image

Figure 6.1: *Reconstruction of an image from the detailed and blurred signals of its projections*

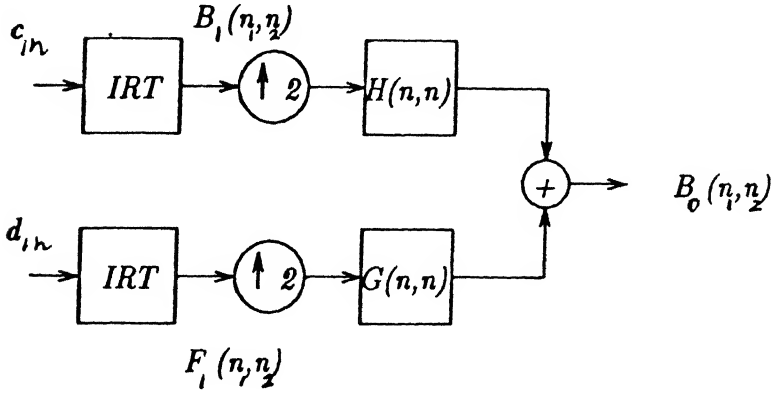

H (n,n) : 2-D Lowpass filter *(refer text for details)*
G (n,n) : 2-D Highpass filter

Figure 6.2: *Modified block diagram*

IRT of c^{θ}_{2n} and d^{θ}_{2n}. In the same way, we can obtain the IRT of the blurred signal $c^{\theta}_{(m-1)n}$ which is the blurred image $B_{(m-1)}(n_1, n_2)$ at the resolution $2^{-(m-1)}$ can be obtained from the IRT of the blurred signal c^{θ}_{mn}, (the blurred image $B_m(n_1, n_2)$) and the IRT of the detailed signal d^{θ}_{mn} (the detailed image $F_m(n_1, n_2)$) at resolution 2^{-m}.

Thus we have outlined a method to hierarchially reconstruct an image from its two dimensional wavelet transform.

6.2 Reconstruction of localised area of interest

An important application of multiresolution reconstruction of the tomographic images, is in reconstructing only the localised region of interest at high resolution with the sorrounding area being reconstructed at a lower resolution to provide a frame of reference. Such a technique may be useful in medical imaging, where a physician may be interested in the cross section of a small region [18]. In [17], Olson et.al., present an algorithm wherein,

- projections at certain angles are exposed only over the localise area of interest;
- one dimensional wavelet transform is applied to each projection to find all of the 1-D wavelet coefficients;
- the low resolution wavelet coefficients for the reduced-exposure projections are replaced with coefficients found by angularly interpolating between the low-resolution wavelet coefficients of the full exposure projections;
- one dimensional inverse wavelet transform is then used to create a complete set of modified projections;
- these modified projections are then used in a standard reconstruction algorithm to arrive at a reconstruction which has high resolution in the region of interest.

The key to their algorithm is that the space-frequency localisation property of compactly supported wavelets (e.g., Daubechies [5]) is essentially preserved after applying the ramp filter used in FBP algorithm [17, 18]. The major drawbacks in their algorithm are listed below.

1. The angular interpolation involved introduces error in the reconstruction [18]. Though, it may not affect the reconstruction at the region of interest, the reconstruction have severe artefacts outside the region of interest.
2. Their algorithm is prone to aliasing error when the region of interest is off centered. The process of centering the projections before interpolation and reconstruction introduces this aliasing error [17].

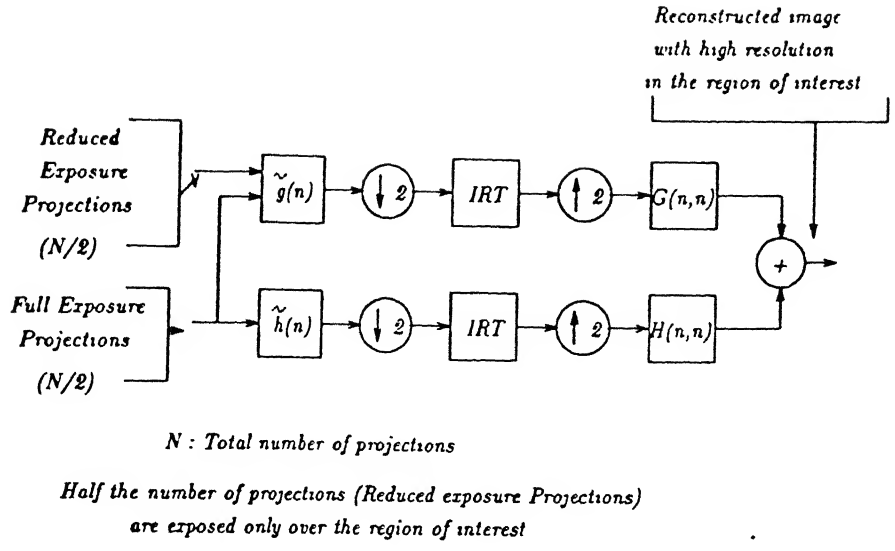

Figure 6.3: *Schematic of the proposed algorithm for 2 levels. The reduced exposure projections are interlaced between the full-exposure projections.*

3. They have not mentioned in their paper how multiple non concentric regions would be handled.

We suggest a modification in their algorithm to overcome these drawbacks. We first note that the main reason for all these problems is the angular interpolation involved. We follow the same radiation exposure pattern suggested by Olson et.al. in [17]. We eliminate the angular interpolation by reconstructing the images at different resolution level from the wavelet transform of the projection using the technique presented in chapter 4. We have proved in chapter 4 that these reconstructed images are the two dimensional wavelet transform of required image. Then we hierarchially reconstruct the final image from their wavelet transform through the method presented in section 6.1. The block diagram of the suggested method for 2 levels is shown in figure 6.3. For a schematic of the radiation exposure pattern refer [17, 18]. The verification of these two suggestions through simulation and if the method is successful, then providing the proper mathematical foundation for it, can be taken up in the future.

Chapter 7

Conclusion

In this thesis work, we had studied some applications of wavelet transform in the area of image reconstruction from projections. An algorithm was proposed to suppress the effect of noise in the reconstructed image from noisy projections using wavelet transform based on spatially variant filtering technique. We demonstrated through simulations, the edge preserving property and the noise suppressing capacity of the proposed technique. We presented a qualitative comparison of our technique with the existing technique on space invariant filtering techniques. We also proved that the images reconstructed from the one dimensional wavelet transform of the projections at a given scale are the two dimensional wavelet transform images of the original image. The two dimensional analysing wavelet is the inverse Radon transform of the 1-D wavelet. The algorithm was implemented to obtain the two dimensional wavelet transform images.

As an extension to the present work, two suggestions were made in chapter 6 for the future work. One deals with reconstructing the image from its wavelet transform obtained by the above method while the other deals with the reconstruction of specific region of interest from essentially localized projections.

Bibliography

[1] Deans S.R., "The Radon Transform and some of its application", *Wiley Interscience Publication*, 1983.

[2] Jain A.K., "Fundamentals of Image Processing", *Prentice Hall International Inc.*, 1989.

[3] Herman G.T., "Image Reconstruction from projections", *Academic Press*, 1980.

[4] Herman G.T., ed., "Image Reconstruction from projections", *Topics in applied physics, Springer Verlag*, 1979.

[5] Daubechies I., "Ten Lectures on Wavelets", *Society for Industrial and Applied Mathematics*, 1992.

[6] Chui C.K., "An Introduction to Wavelets", *Academic Press*, 1992.

[7] Van Trees H.L., "Detection, Estimation and Modulation Theory", Part 1, *John Wiley and Sons*, 1968.

[8] Papoulis A., "Probability, Random Variables and Stochastic Process", third ed., *McGraw Hill Publishers.*

[9] Sahiner B., Yagle A., "Time Frequency Distribution of Radon Transform", *IEEE Transactions on Image Processing*, Vol.2, No.4, October 1993.

[10] Sahiner B., Yagle A., "Image Reconstructions from projections under wavelet constraints", *IEEE Trans. on Signal Processing*, Vol.41, No.12, December 1993.

[11] Noonan J.P., Polchlopek H.M., Varteresian M., "A Hypothesis Testing Technique for Wavelet transform in the presence of Noise", *Digital Signal Processing*, 3, (89-96),1993.

[12] Peyrin F., Zaim M. and Goutte R., "Construction of Wavelet Decompositions for Tomographic Images", *Journal of Mathematical Imaging and Vision*, 3, (105-121) 1993.

[13] Shepp L.A., Logan B.F., "The Fourier Reconstruction of a head section", *IEEE Trans. on Nuclear Science*, Vol 21., June 1974.

[14] Mallat S.G., "A Theory for Multiresolution Signal Decomposition : The Wavelet Representation", *IEEE Trans. on Pattern Analysis and Machine Intelligence*, Vol.11, No.7, July 1989.

[15] Mallat S.G., "Multifrequency Channel Decomposition of Images and Wavelet Models", *IEEE Trans on ASSP*, Vol.37, No.12, December 1989.

[16] Rioul O, Vetterli M., "Wavelets and Signal Processing", *IEEE Signal Processing Magazine*, October 1991.

[17] Olson T., DeStefano J., *Wavelet Localization of the Radon Transform, IEEE Trans on Signal Processing*, Vol.42., No.8, August 1994.

[18] Delaney A.H., Bresler Y., "Multiresolution Tomographic Reconstruction Using Wavelets", *IEEE Trans. on Image Processing*, To appear in 1995.

[19] Cody M.A., "The Fast Wavlet Transform", *Dr.Doob's Journal*, April 1992.

[20] Cody M.A., "The Wavelet Packet Transform", *Dr.Doob's Journal*, April 1994.

Appendix A

We attempted to quantify the error in the reconstruction from noisy projections with the preprocessing technique. The results are presented here. Two error measures are used [3].

$$MSE = \left(\sum_m \sum_n [f(m,n) - t(m,n)]^2 \right)^{\frac{1}{2}} \quad \text{(A.1)}$$

$$NMAD = \frac{\sum_m \sum_n |f(m,n) - t(m,n)|}{\sum_m \sum_n |t(m,n)|} \quad \text{(A.2)}$$

In the above equations,

MSE	:	Mean Square Error
NMAD	:	Normalised Mean Absolute distance
$f(m,n)$	:	Reconstructed image
$t(m,n)$	:	Original image
$\bar{t}$	:	Average value of the original image

The simple square image which is given in the simulation chapter is used. The MSE and $NMAD$ as a function of the variance of the noise added to the projections is plotted in figure A.1 and A.2 for the images,

- reconstructed from noisy projections.
- reconstructed using hamming filter technique.
- reconstructed using the proposed preprocessing technique.

The variance of the noise in the projections is varied from 1×10^{-4} to 36×10^{-4} The error in the image reconstructed from the hamming filter technique is large due to the large deviations near the edges in the image.

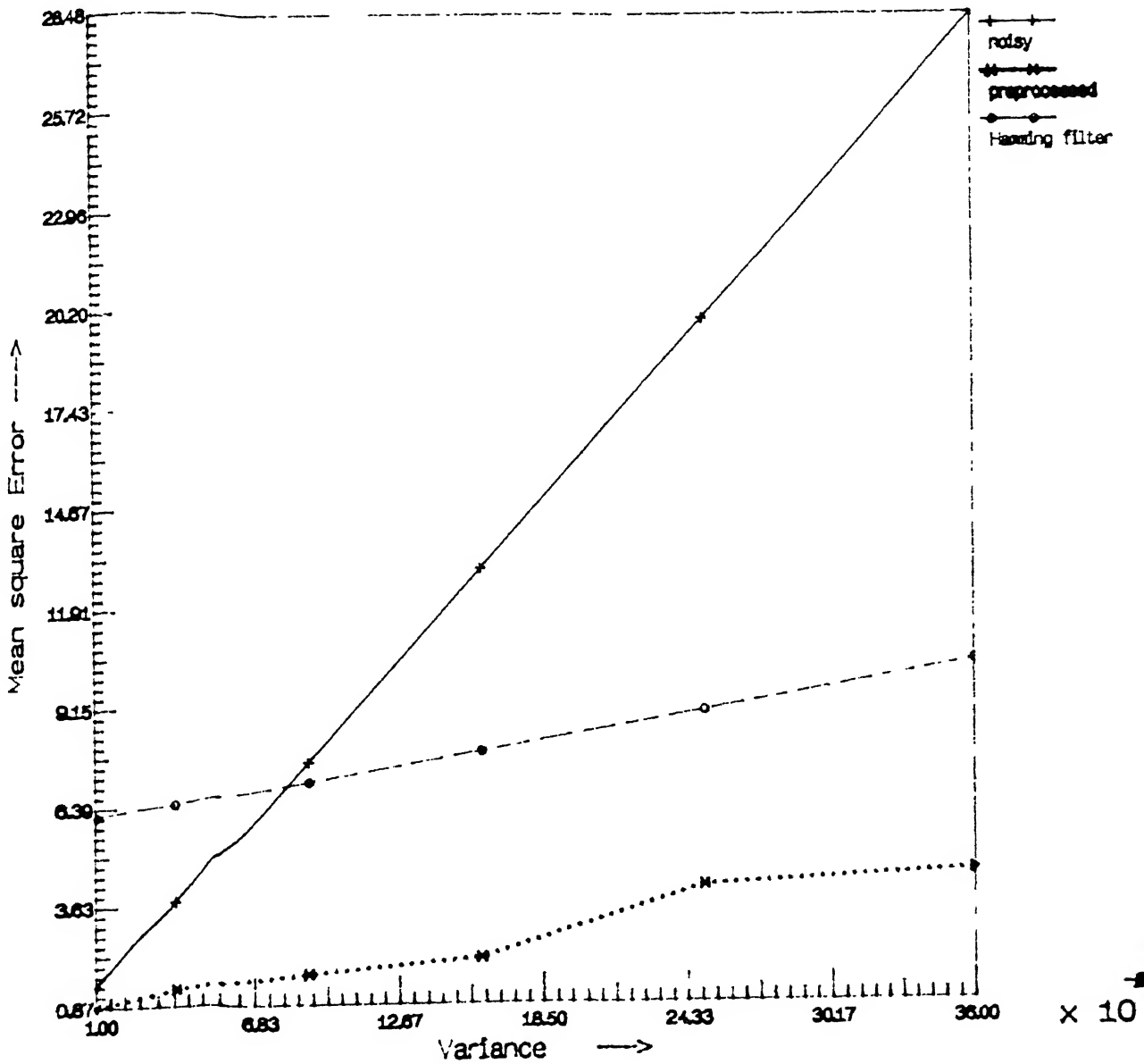

Figure A.1: *MSE vs Noise variance*

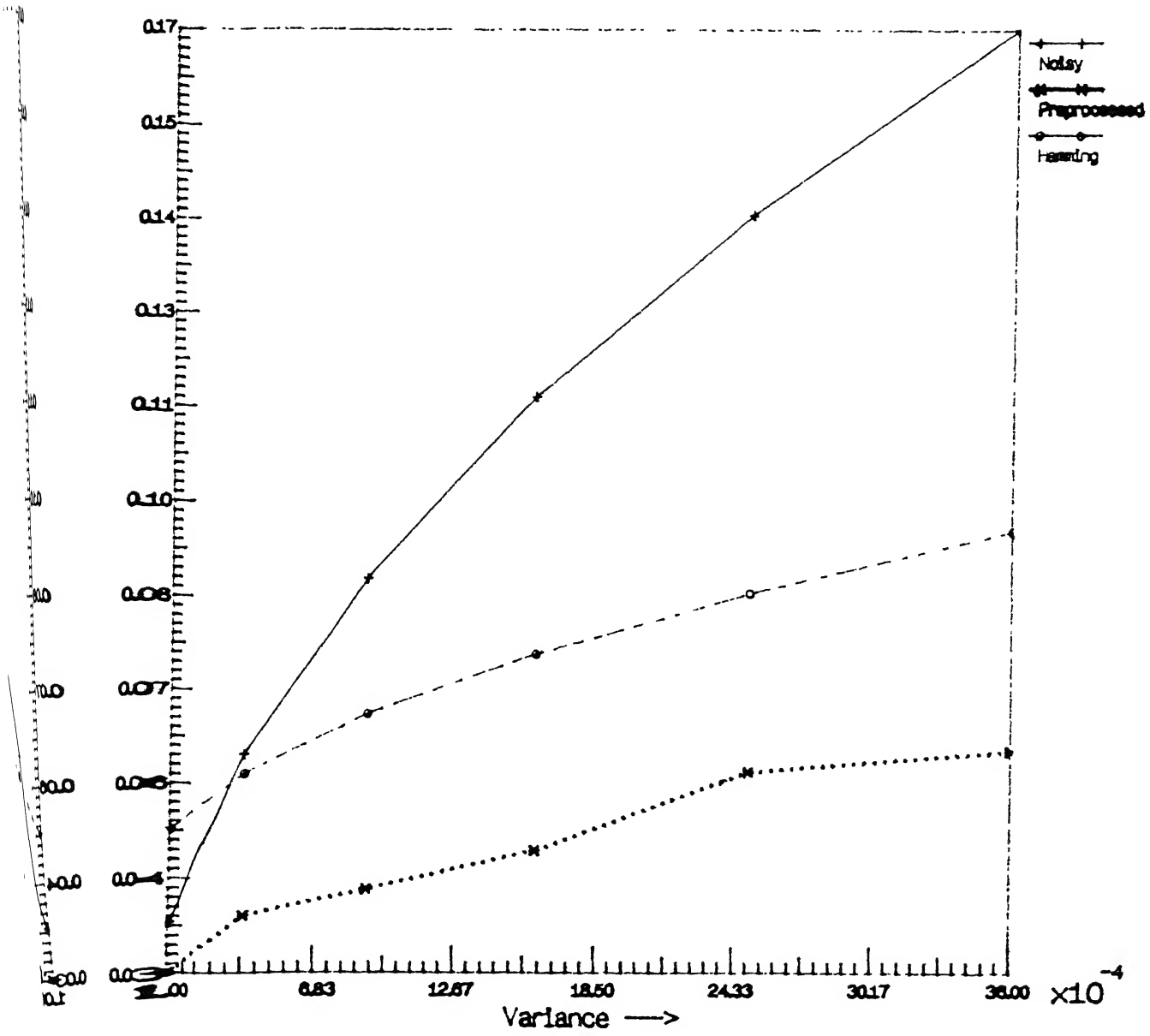

Figure A.2: *Normalised Mean Absolute Distance vs Noise variance*